Appl. Phys. B 76, 173–182 (2003)
DOI: 10.1007/s00340-003-1112-z

Applied Physics B
Lasers and Optics

C. HENKEL[1,✉]
P. KRÜGER[2]
R. FOLMAN[2]
J. SCHMIEDMAYER[2]

Fundamental limits for coherent manipulation on atom chips

[1] Institut für Physik, Universität Potsdam, 14469 Potsdam, Germany
[2] Physikalisches Institut, Universität Heidelberg, 69120 Heidelberg, Germany

Received: 22 August 2002/Revised version: 30 October 2002
Published online: 26 February 2003 •

ABSTRACT The limitations for the coherent manipulation of neutral atoms with fabricated solid-state devices, so-called 'atom chips', are addressed. Specifically, we examine the dominant decoherence mechanism, which is due to the magnetic noise originating from the surface of the atom chip. It is shown that the contribution of fluctuations in the chip wires at the shot-noise level is not negligible. We estimate the coherence times and discuss ways to increase them. Our main conclusion is that future advances should allow for coherence times as long as 1 s, a few μm away from the surface.

PACS 03.75.-b; 32.80.Lg; 03.67.Lx; 05.40.-a

1 Introduction

In the quest for physical implementations of quantum information processing, 'atom chips' are currently of great interest. This is because they promise well-controlled quantum optical manipulations of neutral atoms in integrated and scalable microtrap arrays. In these traps, atoms are strongly confined by electromagnetic fields close to nanostructured solid-state substrates. Microtraps used in current experiments are magnetic traps produced by current-carrying wires [1–10] and periodically magnetized substrates [11], or hybrid traps involving optical or electric fields [12, 13].

In this paper, we discuss the limitations that wire-based magnetic traps on atom chips may have to face when they are down-scaled into the micron range. Recently, both theoretical and experimental indications have been found that the 'hot' chip substrate – typically held at room temperature – is not a quiet environment: at distances below a few hundred μm from the chip, the trap lifetime is shorter than in free space and the atom temperature increases [5, 6, 14–17]. While it is not excluded that strong compression in these microtraps plays a role due to enhanced collisional interactions (see [18] for a review), noisy magnetic fields may also be involved. They provide a coupling to the environment that may cause loss, heating and decoherence and are elaborated upon in this paper. We review the sources of magnetic fields and quote estimates for trapping and coherence times. In particular, we discuss the contribution of electric current noise at the shot-noise level and evaluate its spectral and spatial properties. This is compared to the noise due to the thermal chip substrate.

✉ E-mail: carsten.henkel@quantum.physik.uni-potsdam.de

2 Atom-chip 'building block': the side guide

In the 1930s, Frisch and Segré realized that when a homogeneous magnetic field ('bias field') is superimposed with the field of a straight-wire current, the magnetic field vanishes on a line parallel to the current (see Fig. 1) [19]. In the vicinity of this line, the field increases in a quadrupolar fashion. The height of the field zero is given by

$$h = \frac{\mu_0}{2\pi}\frac{I}{B_\mathrm{b}}\,, \tag{1}$$

where $\mu_0 = 4\pi$ mm G/A is the vacuum permeability, I the wire current and B_b the bias-field magnitude. (This expression applies to finite-size wires provided their diameter $\ll h$.) This 'side guide' can be implemented on an atom chip using a lithographically etched wire on the chip surface. The setup is ideal for miniaturization since the guide height is reduced using smaller currents (with less ohmic dissipation).

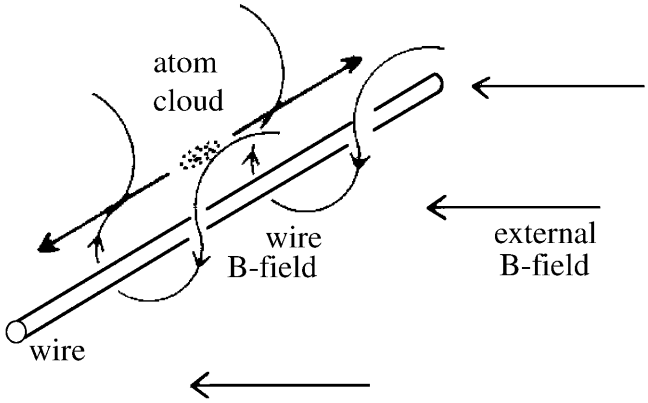

FIGURE 1 Principle of a linear magnetic quadrupole guide ('side guide'). Figure courtesy of Sierk Pötting

Atoms with a nonzero magnetic moment $\boldsymbol{\mu}$ are trapped around the magnetic field minimum provided $\boldsymbol{\mu}$ keeps an antiparallel orientation with respect to the local magnetic field (adiabatic approximation). These 'weak-field seekers' are attracted to the field zero and get trapped in a potential, $\mu_\parallel|\boldsymbol{B}_0(\boldsymbol{x})|$, proportional to the magnitude of the magnetic field. (The subscript 0 distinguishes the static trapping field from the field fluctuations discussed later.) It is particularly interesting to introduce a longitudinal magnetic field (along the wire) so that the field magnitude never reaches zero: this helps satisfying the adiabatic approximation everywhere and reduces so-called 'Majorana flips' into untrapped magnetic sublevels. The trapping potential is then a harmonic well instead of a linear one around the guide center. This is the guide geometry we focus on in the following. The relevant parameters are the trap height h (1), the oscillation frequency $\Omega/2\pi$ in the harmonic well and the Larmor frequency $\omega_\mathrm{L} = \mu_\parallel|\boldsymbol{B}_0(\boldsymbol{r})|/\hbar$, where $\boldsymbol{B}_0(\boldsymbol{r})$ is the field at the trap center and $\mu_\parallel$ is the magnetic moment along the center field [4, 10]. For the lowest quantum states in the potential well, the magnetic field is predominantly longitudinal, and the single-particle wave functions are approximately harmonic oscillator states for quantum numbers up to $n \sim \omega_\mathrm{L}/\Omega$.

The validity of the adiabatic approximation is also determined by the ratio ω_L/Ω: it has been estimated that nonadiabatic losses are exponentially suppressed when this ratio is large [20] (see also [21]). Similarly, tunnelling losses down to the chip surface can be made exponentially small with a sufficiently high and 'thick' potential barrier. The main loss channel is then provided by the uncontrollable coupling to the surface via magnetic noise.

3 Interaction with magnetic noise

3.1 *Noise spectrum and spin-flip rate*

The coupling of the atomic magnetic moment to fluctuating magnetic fields gives rise to both spin flips and changes in the center-of-mass motion (scattering). The rate of these processes is given by Fermi's golden rule. We recall here that it can be conveniently expressed in terms of the noise spectrum of the magnetic field fluctuations. (See [22] for a similar approach and [23, Chap. IV] for the derivation of a full master equation.)

If we write $|i\rangle$ and $|f\rangle$ for the atomic states before and after the transition, the transition rate is

$$\Gamma_{\mathrm{i}\to\mathrm{f}} = \frac{2\pi}{\hbar}\sum_{\mathrm{F,I}} p(I)\,|\langle F,\, f|H_\mathrm{int}|I,\, i\rangle|^2 \times \delta(E_\mathrm{F} + E_\mathrm{f} - E_\mathrm{I} - E_\mathrm{i})\,, \tag{2}$$

where $|I\rangle$ and $|F\rangle$ are initial and final states for the field, the summation being an average over the initial field states (with probabilities $p(I)$) and a trace over the final field states. The interaction Hamiltonian is given by $H_\mathrm{int} = -\boldsymbol{\mu}\cdot\boldsymbol{B}(\boldsymbol{x})$.

Consider first the rate for spin flips. Since only a subset of magnetic sublevels $|m_\mathrm{i}\rangle$ are weak-field seekers, spin flips $|m_\mathrm{i}\rangle \to |m_\mathrm{f}\rangle$ are responsible for trap loss. The magnetic field is evaluated at the position $\boldsymbol{r}$ of the trap center. (An average over the atomic position distribution would be more accurate.) We write the δ-function for energy conservation as a time integral over $\mathrm{e}^{\mathrm{i}(E_\mathrm{I}-E_\mathrm{F}-\hbar\omega_\mathrm{fi})t/\hbar}$, where $\hbar\omega_\mathrm{fi} = E_\mathrm{f} - E_\mathrm{i}$. The exponential $\mathrm{e}^{\mathrm{i}(E_I-E_\mathrm{F})t/\hbar}$ can be removed by introducing the field operators in the Heisenberg picture:

$$\boldsymbol{B}(\boldsymbol{r}, t) = \mathrm{e}^{\mathrm{i}H_0 t/\hbar}\,\boldsymbol{B}(\boldsymbol{r})\mathrm{e}^{-\mathrm{i}H_0 t/\hbar} \tag{3}$$

(here, H_0 is the free-field Hamiltonian) and taking matrix elements of this operator between the initial and final field states. This gives

$$\mathrm{e}^{\mathrm{i}(E_\mathrm{I}-E_\mathrm{F})t/\hbar}\langle I|\boldsymbol{B}(\boldsymbol{r})|F\rangle = \langle I|\boldsymbol{B}(\boldsymbol{r}, t)|F\rangle. \tag{4}$$

The sum over the final states $|F\rangle$ now reduces to a completeness relation and we get (α, β denote field components)

$$\begin{aligned} &2\pi\hbar\sum_{\mathrm{F,I}} p(I)\langle I|B_\alpha(\boldsymbol{r})|F\rangle\langle F|B_\beta(\boldsymbol{r})|I\rangle\delta(E_\mathrm{F} - E_\mathrm{I} - \hbar\omega) \\ &= \int_{-\infty}^{\infty}\mathrm{d}t\,\mathrm{e}^{\mathrm{i}\omega t}\sum_\mathrm{I} p(I)\langle I|B_\alpha(\boldsymbol{r}, t)B_\beta(\boldsymbol{r}, 0)|I\rangle \\ &= S_{\alpha\beta}(\boldsymbol{r};\omega)\,. \end{aligned} \tag{5}$$

In the last line, we have defined the magnetic noise spectrum, which is the Fourier transform of the field's autocorrelation function. The rate for spin flips can now be written as

$$\Gamma_{\mathrm{i}\to\mathrm{f}} = \frac{1}{\hbar^2}\sum_{\alpha,\beta=x,y,z}\langle m_\mathrm{i}|\mu_\alpha|m_\mathrm{f}\rangle\langle m_\mathrm{f}|\mu_\beta|m_\mathrm{i}\rangle S_{\alpha\beta}(\boldsymbol{r}, -\omega_\mathrm{fi})\,. \tag{6}$$

Since $m_\mathrm{f} \neq m_\mathrm{i}$, the matrix elements of μ_α are only nonzero for directions perpendicular to the magnetic field at the trap center. We also recover the selection rule $m_\mathrm{f} - m_\mathrm{i} = \pm 1$, so that the relevant transition frequency is the Larmor frequency $|\omega_\mathrm{fi}| = \omega_\mathrm{L}$. The spin-flip rate gives the order of magnitude of trap loss even if more than one weak-field-seeking Zeeman state, $m_\mathrm{i} = +2, +1$, say, are trapped (possible with many of the alkali atoms). This is because the matrix elements between adjacent sublevels do not significantly differ in magnitude so that the atoms reach the nontrapped sublevel $m_\mathrm{f} = 0$ after a time $\sim 2/\Gamma_{+2\to+1}$.

We finally note that as long as the behavior of the 'environment' (the field) is ignored in the description of the atom's dynamics, the noise spectrum is the only quantity needed to characterize the environment. It is also an experimentally measurable quantity: for example, the rms magnetic noise $\langle B_x^2(\boldsymbol{r})\rangle^{1/2}$ measured by a spectrum analyzer in a given frequency band $\Delta\omega/2\pi$ around ω is $(2S_{xx}(\boldsymbol{r}, \omega)\,\Delta\omega/2\pi)^{1/2}$, the factor 2 accounting for the sum over positive and negative frequencies. The atomic spin-flip rate may be regarded as an alternative way to measure the noise spectrum. In order of magnitude, the magnetic moment is comparable to the Bohr magneton, μ_B ($\mu_\mathrm{B}/2\pi\hbar = 1.4\,\mathrm{MHz/G}$), and we get

$$\Gamma_{\mathrm{i}\to\mathrm{f}}(\boldsymbol{r}) \sim 0.01\,\mathrm{s}^{-1}(\mu/\mu_\mathrm{B})^2\,\frac{S_{\alpha\beta}(\boldsymbol{r}, \omega_\mathrm{L})}{\mathrm{pT^2/Hz}}\,. \tag{7}$$

Note that current SQUID magnetometers are able to detect magnetic field noise even on the $10\,\mathrm{fT}/\sqrt{\mathrm{Hz}}$ scale [24].

3.2 *Near-field noise*

The magnetic noise spectrum close to a solid substrate shows dramatic differences with respect to the well-known black-body spectrum. This is because thermally excited currents in the substrate (Johnson–Nyquist noise) generate electromagnetic fields with substantial nonpropagating components. As an illustration, Fig. 2 shows the noise spectrum at a fixed distance ($h = 1\,\mu\text{m}$) above a metallic half-space, calculated along the lines of [15]. One gets an increase of several orders of magnitude for low frequencies (wavelength λ much larger than h). In addition, the spectrum is rather flat in this range. Only at high frequencies ($\lambda < h$) is the Planck spectrum recovered because the detector then enters the far field of the source.

In the low-frequency range, the magnetic near-field noise above a planar substrate is approximately characterized by the spectrum [15]

$$\frac{\omega h}{c} \ll 1: \quad S_{\alpha\beta}(\boldsymbol{r},\omega) = \frac{\mu_0^2 k_\mathrm{B} T}{16\pi\,\varrho}\,\frac{s_{\alpha\beta}}{h}\left[1+\frac{2\,h^3}{3\,\delta(|\omega|)^3}\right]^{-1}, \quad (8)$$

where T and ϱ are the substrate temperature and resistivity, respectively, h is the observation distance, $s_{\alpha\beta} = \mathrm{diag}(\frac{1}{2}, 1, \frac{1}{2})$ is a diagonal tensor (the distinguished axis is along the surface normal) and $\delta(\omega) = \sqrt{2\varrho/\mu_0\omega}$ is the skin depth. In order of magnitude, the corresponding spin-flip rate is surprisingly large for traps at a micrometer distance:

$$h \ll \delta(\omega_\mathrm{L}): \quad \Gamma_{\mathrm{i}\to\mathrm{f}} \sim 100\,\mathrm{s}^{-1}\,\frac{(\mu/\mu_\mathrm{B})^2 (T/300\,\mathrm{K})}{(\varrho/\varrho_{Cu})(h/\mu\mathrm{m})}, \quad (9)$$

where $\varrho_{Cu} = 1.7\times10^{-6}\,\Omega\,\mathrm{cm}$ is the copper resistivity. The flip rate is plotted as a function of distance in Fig. 3. A larger Larmor frequency (longitudinal bias field) only helps reducing spin flips when $h > \delta(\omega_\mathrm{L})$, giving a scaling $\Gamma_{\mathrm{i}\to\mathrm{f}} \propto \omega_\mathrm{L}^{-3/2}$. Finally, there are many plausible reasons to expect that the linear dependence on T of the flip rate (9) does not continue down to very low temperatures: the full Bose–Einstein occupation number has to be used, $k_\mathrm{B}T \mapsto \hbar\omega_\mathrm{L}\,(1-\mathrm{e}^{-\hbar\omega_\mathrm{L}/k_\mathrm{B}T})^{-1}$, and other sources of magnetic fields may come into play like

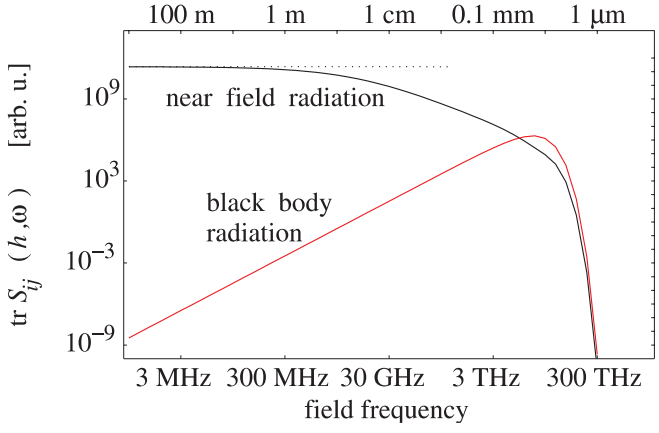

FIGURE 2 Magnetic near-field noise spectrum. The near-field spectrum is calculated along the lines given in [15]. The source is a copper half-space at $T = 300\,\mathrm{K}$, observation distance $h = 1\,\mu\mathrm{m}$. The trace of the magnetic correlation tensor is shown. The *top labels* give the wavelength λ

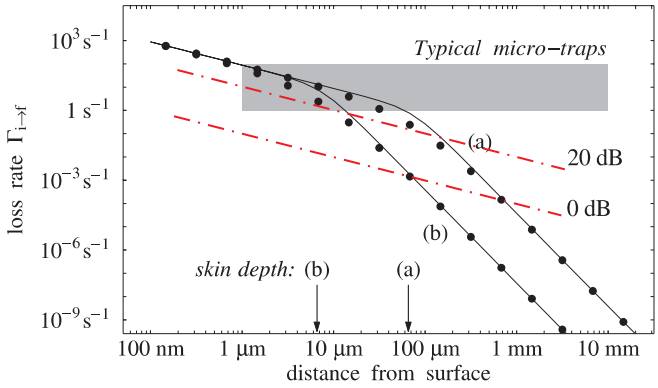

FIGURE 3 Rate of spin flips in a microtrap above a planar metal substrate. The *black solid lines* describe the near-field noise generated by thermally excited currents (Johnson noise) in the substrate, as given by (8). The *dots* are an exact numerical calculation from [15]. Larmor frequencies $\omega_\mathrm{L} = \mu_\mathrm{B}|\boldsymbol{B}(\boldsymbol{r})|/\hbar = 1\,\mathrm{MHz}\times 2\pi$ (**a**) and $100\,\mathrm{MHz}\times 2\pi$ (**b**) are chosen. The *red dash-dotted lines* describe the noise due to fluctuations in the electric current of a side guide. The current noise is assumed at shot-noise level (0 dB) or 20 dB above shot noise. The guide height h is lowered by ramping down the wire current I with a constant ratio I/h and at fixed bias field $B_\mathrm{b} = 100\,\mathrm{G}$, cf. (1)

spin waves, lattice vibrations, etc. One thus probably gets lifetimes (and coherence times, see the following) shorter than predicted by (9).

At room temperature, the estimate (9) describes a worst case because most materials have a resistivity larger than copper. A structured substrate like a thin metallic layer or a wire also helps: the magnetic noise then decreases more rapidly with distance h [10, 25]. As a general rule, the smaller the amount of metallic material, the lower the magnetic noise. This can be understood from a simple model where thermally excited currents in each volume element of the conducting substrate contribute to the total magnetic noise above (a similar approach has been used in [24, 26]). For distances $h \ll \delta(\omega)$, one obtains a noise spectrum accurate within a factor of two from an incoherent addition of magnetostatic fields, neglecting the influence of the material on the field propagation. For example, at a distance h from a single, thin wire with radius $a \ll h$, the theory of [25] yields a magnetic noise tensor given by (8) with the replacement $s_{\alpha\beta}/h[1+\ldots]^{-1} \mapsto (\pi a^2/h^3)\mathrm{diag}(2, \frac{1}{2}, \frac{3}{2})$, showing a similar weak anisotropy. The components specify the azimuthal, radial and longitudinal directions in cylindrical coordinates, respectively. The correction involving the skin depth $\delta(\omega)$ cannot be obtained in the magnetostatic approximation.

Experimental data [5–7, 16] indicate that trap lifetimes as long as or even longer than estimated by (9) (several hundred ms to 100 s) are achievable: these traps were built close to thin wires (3- to 90-μm width) or semiconductor substrates covered with thin metallic layers (thickness $\ll h$), at distances between 20 μm and 2 mm. It should be noted that the distance dependence of the trap lifetime measured in [16] only agrees qualitatively with our theory, and more detailed investigations are required.

3.3 *Current noise*

The electric currents that generate the side-guide fields are also subject to fluctuations that drive spin flips and

deform the trapping fields. The impact of technical noise can be reduced using electronic filtering, 'quiet' drivers, by correlating the currents for the wire and the bias field, etc. This works down to the most fundamental level where the noise due to the discrete value of the electron charge comes into play ('shot noise'). For a current I in free space, shot noise has a frequency-independent spectrum given by

$$SN_{\mathrm{I}} = eI \approx 0.16\,\mathrm{nA^2/Hz}\,\frac{I}{\mathrm{A}}, \tag{10}$$

where e is the charge quantum. Note that currents in a solid wire can have fluctuations below the shot-noise limit because the Coulomb interaction correlates the electrons. In the following, we use SN_{I} as a convenient reference value.

If the wire current in a side guide has a noise spectrum $S_{\mathrm{I}}(\omega)$, it creates a magnetic field with

$$S_{\mathrm{B}}(\boldsymbol{r},\omega) = \frac{\mu_0^2 eI}{4\pi^2\hbar^2}\,\frac{S_{\mathrm{I}}(\omega)}{SN_{\mathrm{I}}}. \tag{11}$$

This scalar quantity gives the azimuthal component of the noise tensor. The spin-flip rate is then of the order of

$$\Gamma_{\mathrm{i}\to\mathrm{f}} \sim 1\,\mathrm{s^{-1}}\,\frac{(\mu/\mu_{\mathrm{B}})^2}{(h/\mu\mathrm{m})^2}\,\frac{S_{\mathrm{I}}(\omega_{\mathrm{L}})}{SN_{\mathrm{I}}}\,\frac{I}{\mathrm{A}}. \tag{12}$$

We conclude that miniaturization beyond the micrometer scale requires extremely low current noise to achieve trap lifetimes longer than seconds. It may well turn out that very large scale atom-chip integration is only possible with static magnetic fields, generated by magnetized nanostructures [11]. Experimental trap lifetime data [5, 16] show that currently used power supplies are quiet enough not to reduce lifetimes at distances above $\sim 10\,\mu\mathrm{m}$.

4 Spin coherence

Coherent manipulation on atom chips requires both that atoms stay trapped and that their quantum state be preserved. Here, we focus on the influence of magnetic noise on the internal (spin) states. For example, different magnetic sublevels or hyperfine states are interesting candidates to implement a bit of quantum information (qubit). Noise-induced transitions between sublevels erase the qubit, and this occurs on the same timescale as the spin flips discussed in the previous section. But the information contained in quantum superpositions can also be lost by pure 'dephasing', without changing sublevel populations [27]. For this process, which opens an additional channel for decoherence, longitudinal magnetic fields, i.e. polarized along the static trapping field ('phase noise'), come into play.

Consider two magnetic sublevels $|m_1\rangle$ and $|m_2\rangle$ that are simultaneously trapped. A magnetic field fluctuation parallel to the static trapping field changes the energy difference between the two qubit states by

$$\Delta E(t) = \Delta\mu_{\parallel} B_{\parallel}(\boldsymbol{r},t)\,, \tag{13}$$

where $B_{\parallel}$ is the longitudinal magnetic field and $\Delta\mu_{\parallel} = \langle m_2|\mu_{\parallel}|m_2\rangle - \langle m_1|\mu_{\parallel}|m_1\rangle$ the differential magnetic moment. (This difference can be substantially reduced in alkalis by choosing hyperfine states that only differ in the nuclear spin state.) Let us now expose a superposition of $|m_1\rangle$ and $|m_2\rangle$ to pure magnetic phase noise during an interaction time t. The off-diagonal element of the corresponding 2×2 density matrix is then proportional to [27]

$$\left\langle \exp\frac{-\mathrm{i}}{\hbar}\int_0^t \mathrm{d}t'\,\Delta E(t')\right\rangle = \exp\left[-\frac{\Delta\mu_{\parallel}^2 t}{2\hbar^2}S_{\parallel}(\boldsymbol{r};0)\right], \tag{14}$$

where $S_{\parallel}(\boldsymbol{r};0)$ is the low-frequency limit of the magnetic noise spectrum. (More precisely, one needs the spectrum averaged over the frequency range 0 to $1/t$. We neglect this complication since the relevant spectra are flat in this range.)

From (14), we conclude that dephasing leads to exponential decoherence of qubit superpositions with a rate similar to the spin-flip rate (cf. (6)). The decoherence rate gets smaller when the logical states have the same magnetic moment (reducing $\Delta\mu_{\parallel}$), or when the magnetic field component $B_{\parallel}$ shows much less noise.

Near-field noise is rather isotropic, as shown by the spectrum (8), and therefore contributes equally to spin flips and phase noise. Noise in the wire current gives only fluctuations perpendicular to the guide axis, so that dephasing is suppressed close to the guide center. Note that this suppression is not complete because of the finite, transverse width of the trapped wave function. In addition, gravity can displace the actual trap center with respect to the magnetic field minimum (the 'gravitational sag' familiar from Bose condensates in magnetic traps, see also [7]). In the harmonic approximation, a simple calculation leads to a reduction of the dephasing rate by a factor $(Mg/\mu_{\parallel}b)^2$, where in order of magnitude

$$\frac{Mg}{\mu_{\parallel}b} \sim 0.1\,\frac{(M/\mathrm{amu})[g/(10\,\mathrm{m/s^2})]}{(\mu_{\parallel}/\mu_{\mathrm{B}})[b/(\mathrm{G/cm})]}\,. \tag{15}$$

This ratio can be made quite small ($< 10^{-6}$) using typical magnetic gradients $b = B_{\mathrm{b}}/h$ achievable with the side guide. Magnetic near fields thus remain as the main source of dephasing noise, with a rate basically scaling like the spin-flip rate.

5 Vibrational coherence

In this section, we turn to scattering processes that leave the atoms in the magnetic trap, but perturb their center-of-mass motion. This occurs whenever the magnetic noise is not spatially homogeneous. A simple model is suggested showing that the typical length scale for magnetic inhomogeneities is of the order of the trap height h for both near-field noise and current noise at the shot-noise level. We discuss the relation between random changes in the atoms' momentum and the decoherence of their density matrix in position space.

5.1 *Scattering rate*

We again use Fermi's golden rule (2), but now the initial and final states are given by wave functions $\psi_{\mathrm{i,f}}(\boldsymbol{x})$. In the following, we retain only a single trapped magnetic sublevel $|m_{\mathrm{f}}\rangle = |m_{\mathrm{i}}\rangle$ and assume that the magnetic moment has the same orientation for all relevant center-of-mass states. Its

matrix elements then reduce to $\mu_\parallel$ (the component along the trapping field). Writing out the overlap integral between wave functions, the transition rate (2) becomes

$$\Gamma_{\mathrm{i}\to\mathrm{f}} = \frac{\mu_\parallel^2}{\hbar^2}\int \mathrm{d}^3x\,\mathrm{d}^3x'\; M_{\mathrm{fi}}^*(\boldsymbol{x})M_{\mathrm{fi}}(\boldsymbol{x}')S_\parallel(\boldsymbol{x},\boldsymbol{x}';-\omega_{\mathrm{fi}})\,, \qquad (16)$$

where the wave-function overlap is given by

$$M_{\mathrm{fi}}(\boldsymbol{x}) = \psi_{\mathrm{f}}^*(\boldsymbol{x})\,\psi_{\mathrm{i}}(\boldsymbol{x})\,, \qquad (17)$$

the transition energy $\hbar\omega_{\mathrm{fi}}$ is the difference between the center-of-mass levels and the field correlation spectrum is the generalization of the noise spectrum (5):

$$S_\parallel(\boldsymbol{x},\boldsymbol{x}';\omega) = \int_{-\infty}^{\infty}\mathrm{d}t\;\mathrm{e}^{\mathrm{i}\omega t}\sum_{\mathrm{I}} p(I)\langle I|B_\parallel(\boldsymbol{x},t)B_\parallel(\boldsymbol{x}',0)|I\rangle\,. \qquad (18)$$

A useful figure that can be extracted from this function is the correlation length l_{c} that governs the variation of (18) as a function of distance $\boldsymbol{s} = \boldsymbol{x}-\boldsymbol{x}'$. As a general rule, one has $S_\parallel(\boldsymbol{x},\boldsymbol{x}';\omega)\to 0$ if $s \gg l_{\mathrm{c}}$ because the fields $B_\parallel(\boldsymbol{x},t)$ and $B_\parallel(\boldsymbol{x}',t)$ become decorrelated. More quantitatively, we define here l_{c} by the following expansion for small deviations from the trap center $\boldsymbol{r}$:

$$S_\parallel(\boldsymbol{x},\boldsymbol{x}';\omega) \approx S_\parallel(\boldsymbol{r};\omega)\left[1-\frac{(\boldsymbol{x}-\boldsymbol{x}')^2}{l_{\mathrm{c}}^2}\right] \qquad (19)$$

provided $\quad |\boldsymbol{x}-\boldsymbol{r}|,\ |\boldsymbol{x}'-\boldsymbol{r}| \ll l_{\mathrm{c}}\,.$

In Sect. 7, we show that the correlation length l_{c} is comparable to the trap height h, for both near-field and current noise.

5.2 *Heating*

Consider the vibrational motion along one transverse direction (the x axis, say) in the harmonic region of the side guide. Magnetic noise can induce transitions between different quantum states in the trap ('heating'). The transition $0\to 1$ between the ground and first excited states is particularly interesting and involves the overlap integral ($\omega_{\mathrm{fi}} = \Omega$)

$$\int \mathrm{d}x\,\mathrm{d}x'\; M_{\mathrm{fi}}^*(x)M_{\mathrm{fi}}(x')S_\parallel(\boldsymbol{x},\boldsymbol{x}';-\Omega) \approx \frac{a^2}{l_{\mathrm{c}}^2}S_\parallel(\boldsymbol{r};-\Omega)\,, \qquad (20)$$

where $a = (\hbar/2M\Omega)^{1/2}$ is the (rms) size of the trap ground state (M is the atomic mass) and the noise spectrum is evaluated at the trap center $\boldsymbol{r}$. Equation (20) is derived in the limit of strong confinement (a much smaller than the correlation length l_{c}), using the expansion (19).

Comparing (20) to (6), we conclude that heating in tight traps is suppressed relative to spin flips, due to the small ratio $(a/l_{\mathrm{c}})^2 \ll 1$. We stress that this is not due to the increase in the trap frequency (because the noise is essentially white), but due to the small size of the trap ground state. Since $l_{\mathrm{c}} \sim h$, the excitation rate $\Gamma_{0\to 1}$ follows power laws $1/h^3$, $1/h^4$, instead of the flip rates (9), (12), depending on the noise source. For example, the rate due to near-field noise above a metallic half-space scales like [10]

$$\Gamma_{0\to 1} \simeq \frac{1\ \mathrm{s}^{-1}\,(\mu/\mu_{\mathrm{B}})^2(T_s/300\ \mathrm{K})}{(M/\mathrm{amu})(\Omega/2\pi\ 100\ \mathrm{kHz})(\varrho/\varrho_{\mathrm{Cu}})(h/\mu\mathrm{m})^3}\,. \qquad (21)$$

Heating is also relevant for the decoherence of qubits implemented in different vibrational levels. One can derive a master equation for the density matrix in the harmonic well that shows that the corresponding off-diagonal elements decay at a rate comparable to $\Gamma_{0\to 1}$. For details, see [15, 26].

Finally, we note that even spatially homogeneous magnetic fluctuations can induce heating when they change the trap position or curvature. Displacing the trap is equivalent to a force and drives the transition $0\to 1$ with a rate [10, 28, 29]:

$$\Gamma_{0\to 1} = \frac{M\Omega^3}{2\hbar}S_h(-\Omega)\,, \qquad (22)$$

where M is the atomic mass and $S_h(\omega)$ is the spectrum of the trap-height fluctuations. Taking into account only field fluctuations caused by the wire current, we get in order of magnitude

$$\Gamma_{0\to 1} \sim 3\ \mathrm{s}^{-1}(M/\mathrm{amu})(\Omega/2\pi\ 100\ \mathrm{kHz})^3\frac{I/\mathrm{A}}{(B_{\mathrm{b}}/\mathrm{G})^2}\frac{S_{\mathrm{I}}(\Omega)}{SN_{\mathrm{I}}}\,. \qquad (23)$$

This rate is still reasonably small for sufficiently large bias fields $B_{\mathrm{b}} > 50$ G. Note, however, that a very strong confinement may not be possible due to the increase with the trap frequency Ω: this occurs because a larger spring constant $M\Omega^2$ translates position fluctuations into larger forces.

Fluctuations in the trap position due to technical noise can be reduced by correlating the currents in the wire with those producing the bias fields. The trap curvature, however, then still fluctuates and changes the oscillation frequency Ω. This gives a parametric resonance on the $0\to 2$ transition with a rate [10, 28, 29]:

$$\Gamma_{0\to 2} = \frac{1}{2}\,S_\Omega(-2\Omega) \qquad (24)$$

$$\sim 3\times 10^{-8}\ \mathrm{s}^{-1}\,\frac{(\Omega/2\pi\ 100\ \mathrm{kHz})^2}{I/\mathrm{A}}\,\frac{S_{\mathrm{I}}(2\Omega)}{SN_{\mathrm{I}}}\,, \qquad (25)$$

which is substantially smaller than the rate (23). Fluctuations in Ω also induce phase noise on the quantum states in the harmonic trap because their energy difference is $\hbar\Omega$. Arguing as in Sect. 4, one finds a dephasing rate comparable to $\Gamma_{0\to 2}$.

In experiments with trapped atoms, it is relatively simple to observe the rate of temperature increase, $\dot{T}$. In the harmonic approximation, one finds a 'heating rate' $k_{\mathrm{B}}T = \hbar\Omega\Gamma_{0\to 1}$ for noise driving the transitions $n\to n\pm 1$ [28, 29]. Currently observed values are in the range of 0.05–1 μK/s [5, 16]. This is orders of magnitude larger than predicted by (21) and excludes an origin dominated by near-field noise. Heating can probably be attributed to current fluctuations, as given by (23), assuming typical power-supply noise spectra (above shot noise). Ambient electromagnetic noise ('electrosmog') may also play a role and is currently under investigation.

6 Spatial coherence

6.1 *Scattering 'cross section'*

We now consider the quasi-free motion along the side-guide axis Oz; the transverse motion is assumed to be 'frozen out'. Noise induces scattering $p_\mathrm{i} \to p_\mathrm{f}$ between different momentum states, where the wave-function overlap $M_\mathrm{fi}(z) = L^{-1}\exp(-\mathrm{i}q_\mathrm{fi}z)$ involves the wavevector transfer $\hbar q_\mathrm{fi} = p_\mathrm{f} - p_\mathrm{i}$ (L is a normalization length). The transition frequency is $\omega_\mathrm{fi} = q_\mathrm{fi}p_\mathrm{i}/M + \hbar q_\mathrm{fi}^2/2M$. We end up with the spatial Fourier transform of the correlation function (the vectors $\boldsymbol{x}, \boldsymbol{x}'$ only differ in their z components):

$$\begin{aligned}\Gamma_{\mathrm{i}\to\mathrm{f}} &= \frac{\mu_\parallel^2}{\hbar^2}\int\frac{\mathrm{d}z\,\mathrm{d}z'}{L^2}\,\mathrm{e}^{\mathrm{i}q_\mathrm{fi}(z-z')}S_\parallel(\boldsymbol{x},\boldsymbol{x}';-\omega_\mathrm{fi})\\ &\approx \frac{\mu_\parallel^2}{\hbar^2}S_\parallel(\boldsymbol{r};-\omega_\mathrm{fi})\int\frac{\mathrm{d}s}{L}\,\mathrm{e}^{\mathrm{i}q_\mathrm{fi}s}C(s;-\omega_\mathrm{fi})\,. \end{aligned}\tag{26}$$

To perform the last step, we have assumed that the correlations involve only the distance $s = z - z'$ (statistically homogeneous noise) and used the normalized correlation function ($C(0;\omega)\equiv 1$):

$$C(z-z';\omega) = \frac{S_\parallel(\boldsymbol{x},\boldsymbol{x}';\omega)}{S_\parallel(\boldsymbol{r};\omega)}\,.\tag{27}$$

Finally, we get a transition rate per wavevector transfer $\mathrm{d}\Gamma/\mathrm{d}q$ by dividing by the wavevector spacing $\mathrm{d}q = 2\pi/L$ in the quantization volume:

$$\frac{\mathrm{d}\Gamma_{\mathrm{i}\to\mathrm{f}}}{\mathrm{d}q} = \gamma\int\frac{\mathrm{d}s}{2\pi}\,\mathrm{e}^{\mathrm{i}q_\mathrm{fi}s}C(s;-\omega_\mathrm{fi})\,,\tag{28}$$

where the rate γ is the prefactor of the integral in (26). If the elements of the magnetic noise tensor are of comparable magnitude, this rate is of the same order as the spin-flip rate (6). As mentioned at the end of Sect. 4, this is the case for near-field noise and to some extent also for fluctuations due to current noise.

We conclude from the differential scattering rate (28) that typical momenta exchanged with the noise field have a magnitude $q_\mathrm{fi} \sim \hbar/l_\mathrm{c}$ given by the inverse noise correlation length.

6.2 *Decoherence*

The relation to spatial decoherence of the atoms has been made more quantitative in [25], where the following master equation for the density matrix $W(z,\,p)$ in the Wigner representation is derived:

$$\left(\partial_t + \frac{p}{M}\partial_z\right)W(z,\,p) = \int\mathrm{d}q\,\frac{\mathrm{d}\Gamma}{\mathrm{d}q}\big(W(z,\,p+\hbar q) - W(z,\,p)\big)\,.\tag{29}$$

The scattering integral on the right-hand side describes processes $p \leftrightarrow p+\hbar q$, while the left-hand side gives the free ballistic motion along the guide axis.

The master equation (29) can be solved exactly using the fact that the 'scattering cross section' (28) is essentially independent of the transition frequency ω_fi for the relevant magnetic field fluctuations. One finds the following expression for the spatially averaged coherence function of the atoms [25]:

$$\begin{aligned}\varrho(s,t) &\equiv \int\mathrm{d}z\langle\psi^*(z+s,t)\psi(z,t)\rangle &(30)\\ &= \varrho(s,0)\exp\big(-\gamma t\,[1-C(s;0)]\big)\,, &(31)\end{aligned}$$

where the brackets denote the average with respect to the noise and $C(s;0)$ is the low-frequency limit of the noise correlation function.

From the coherence function (31), we identify $\gamma[1-C(s;0)]$ as the decoherence rate for spatially separated superposition states: for a splitting greater than the correlation length, $s \gg l_\mathrm{c}$, the correlation function $C(s;0)$ is zero and the superposition decays into a statistical mixture on a timescale given by $1/\gamma$, comparable to the spin lifetime. Superpositions with smaller splitting s decay more slowly, with a rate scaling like $[1-C(s;0)]\gamma \approx (s/l_\mathrm{c})^2\gamma \ll \gamma$, using the expansion (19). This behavior was also found in a decoherence model by Zurek [30], who used a master equation in Fokker–Planck form instead of our (29).

We note that the decoherence rate just found also describes the dephasing between the arms of a guided matter wave interferometer [10, 31, 32]. This follows from an argument similar to that used in (14). In this context, s is the (transverse) separation between the arms of the interferometer. For more details, we refer the reader to [10].

6.3 *Decoherence of a condensate*

We now discuss the extension of the previous results to the case of a Bose condensate in a linear waveguide (see [9] for a review of experiments). The single-particle wave functions then have to be replaced by collective modes, and the effective potential is changed due to atom–atom interactions. For example, the (transverse) ground state has a larger width compared to the single-particle wave function, so that the atomic spins are no longer aligned along the guide axis. We present here preliminary results for the decoherence of a Bose condensate focussing on a quasi-one-dimensional regime [33–36]. Adopting a mean-field description, we have performed Monte Carlo simulations of the one-dimensional Gross–Pitaevski equation

$$\mathrm{i}\hbar\frac{\partial\psi}{\partial t} = -\frac{\hbar^2}{2M}\frac{\partial^2\psi}{\partial z^2} + V(z,t)\psi + g|\psi(z)|^2\psi\,,\tag{32}$$

where the coupling constant $g = 2\hbar\Omega a_\mathrm{s}$ is proportional to the (transverse) trap frequency and the s-wave scattering length $a_\mathrm{s} > 0$ (repulsive interactions). The random potential $V(z,t)$ is chosen in accordance with the correlation functions relevant for atom-chip traps (white noise and Lorentzian spatial correlations). The initial situation is a condensate in the ground state of a harmonic trap superimposed on the waveguide potential. Quantum (phase) fluctuations [35, 36] are ignored, assuming effectively $T_{at} = 0$. The harmonic confinement is instantaneously released at $t = 0$, and the cloud expands along the waveguide axis.

The simulation results given in Fig. 4 show the spatially averaged coherence function of the condensate, (30), as a function of the separation s for different expansion times t. One observes that in the presence of noise (scattering rate

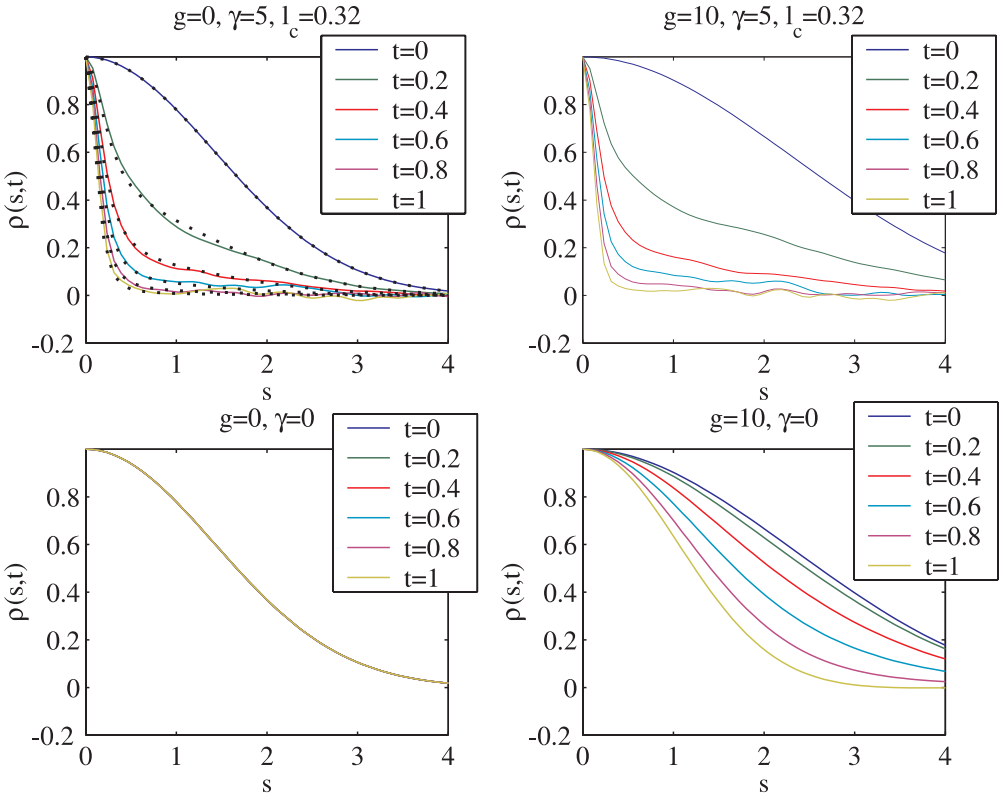

FIGURE 4 Spatially averaged coherence function (30) of a condensate expanding in a noisy waveguide. *Upper row*: with noise giving a total scattering rate $\gamma = 10$ and correlation length $l_c = 1/\sqrt{10}$. *Lower row*: no noise ($\gamma = 0$). *Left column*: noninteracting cloud ($g = 0$), *right column*: with interactions ($g = 10$). The *dotted lines* in the *upper left panel* are the analytical prediction (31). The units are harmonic oscillator units relative to the initial confinement along the guide axis

$\gamma \neq 0$), the coherence length (the width of $\varrho(s, t)$) is reduced as time increases – the cloud breaks apart in mutually incoherent patches that have 'seen' different noise potentials. The dotted lines in the upper left figure give the prediction (31) of the master equation for noninteracting atoms, and we note a very good agreement between the analytics and the numerical data.

We find that the decoherence scenario is not qualitatively changed by a moderate self-interaction, as a comparison of the panels for $g = 0$ and $g = 10$ shows. Only for short times is the coherence length of an interacting cloud larger because the ground state is broadened by the interactions. A more detailed investigation of condensate decoherence, including analytical approximations and the limit of strong interactions, will be presented elsewhere [37].

7 Noise correlation length

We finally show that magnetic noise involved in atom chips has a correlation length $l_c \sim h$, for both near-field and current noise.

7.1 *Near-field noise*

The spatial correlation function for the electric near field above a thermal, planar substrate was studied in [38]. A similar calculation yields for the magnetic near field the following normalized correlation function:

$$C(s;0) = \frac{8h^2}{(2h+\sqrt{s^2+4h^2})\sqrt{s^2+4h^2}} \approx \frac{16h^2/3}{s^2+16h^2/3}\,. \tag{33}$$

This gives the correlation for the magnetic field component $B_\parallel$, taken at positions z, z' on the side-guide axis with a separation s. We have assumed that the field wavelength (fixed by the transition frequency $\omega_{\rm fi}$) is much larger than the relevant distances s, h. The Lorentzian form in (33) is a good approximation for all distances where $C(s; 0)$ is sensibly nonzero and shows even more explicitly that the correlation length is of the order of the guide height h. This is because the noise fields radiated by each volume element of the substrate are quasi-static in the near field and decay algebraically (no retardation).

7.2 *Shot-noise correlations*

One might think at first sight that magnetic noise due to current fluctuations should have a large correlation length because the relevant electromagnetic frequencies (kHz to MHz range) propagate with a large wavelength along the wire. The analysis of near-field fluctuations has shown, however, that the wavelength is not really the relevant scale as soon as one is sensitive to nonpropagating fields generated by nearby sources. For this reason, we suggest a simple toy model for the flow of electrons through a thin wire that allows us to recover both the noise spectrum of the magnetic field and its spatial correlations.

The ingredients of the model are sketched in Fig. 5 and details are given in Appendix A. The electrons are assumed to move independently and ballistically (the Drude electron-gas model); their transverse position in the wire is neglected compared to the guide distance h. It is beyond the scope of this model to describe correlations between the electrons that could lead to lower current fluctuations. Neither does the

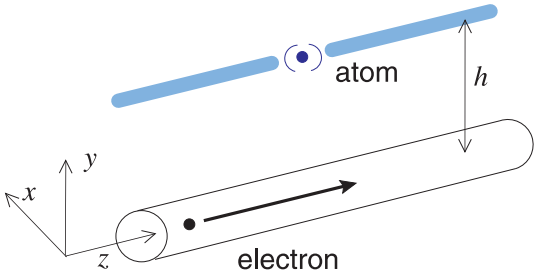

FIGURE 5 Model for shot noise: ballistic electron flow

model describe diffusive electron transport; we comment on that below.

The result of the model is the magnetic noise spectrum (A.5) given in the appendix. We recover the previous spectrum (11) (with current noise at the shot-noise level, $S_I(\omega) = SN_I$) in the low-frequency limit where $\omega h \ll v$ for all relevant electron velocities v. At high frequencies, the noise is reduced because one needs fast electrons to produce magnetic field 'pulses' with short duration $\sim h/v$. This is visible in Fig. 6, where the spectrum (A.5), for fixed $h = 1\,\mu\text{m}$, is shown as a function of frequency, normalized to its low-frequency limit. The high-frequency cutoff occurs at $\omega h \gg v_F$, where v_F is the Fermi velocity when the Fermi–Dirac distribution is taken for $P(v)$. A Maxwellian distribution gives a similar behavior with a lower cutoff, as shown in the figure. Note again that at most frequencies relevant for atom-chip traps, the noise spectrum can be assumed flat.

The characteristic length scale l_c for the spatial correlation of the shot-noise fields can also be read off from (A.5). In the directions perpendicular to the guide axis, it is given by the guide height h, and we recover the same correlation length as for near-field fluctuations. For the motion along the guide axis, the simplest way is compute the differential scattering rate (28). For a process $p_i \to p_i + \hbar q$, we get

$$\frac{\mathrm{d}\Gamma_{i\to f}}{\mathrm{d}q} = \gamma_{SN}\frac{p_i}{Mq}P(p_i/M)\,[qhK_1(qh)]^2\,, \tag{34}$$

where we have neglected the recoil shift $\hbar q^2/2M$ compared to the Doppler shift qp_i/M. The scattering rate is

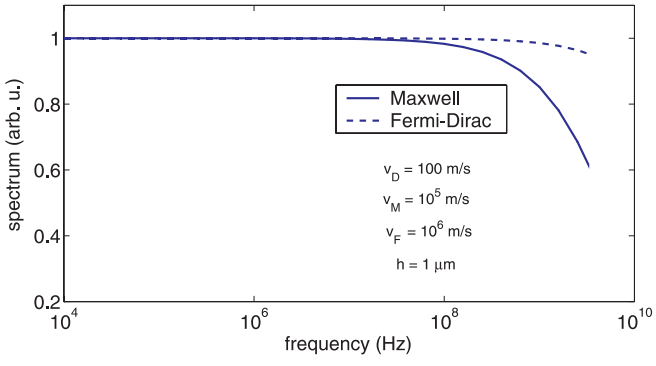

FIGURE 6 Magnetic noise spectrum (A.5) from the ballistic electron model. The spectrum is taken at the side-guide center (height $h = 1\,\mu\text{m}$) and normalized to its low-frequency limit. The electron velocity distribution $P(v)$ is that of Maxwell or Fermi–Dirac with characteristic velocities as given in the figure. The distribution is centered around the drift velocity v_D

$$\gamma_{SN} = \frac{\mu_\parallel^2\cos^2\alpha}{\hbar^2}\frac{\mu_0^2 eI}{4\pi^2h^2}\,, \tag{35}$$

where α is the angle between the atomic spin and the wire field. If the harmonic approximation for the transverse motion is not valid, $\cos\alpha$ is not small and (35) is comparable to the spin-flip rate (cf. (11)), typically a few $1\,\text{s}^{-1}$. K_1 in (34) is the modified Bessel function of the second kind, and $P(v)$ is the electrons' velocity distribution, taken at the atomic velocity p_i/M. It is interesting that the scattering involves a class of electrons co-moving with the atom: this suggests that the atomic wave in the linear guide is diffracted by the spatially confined field pulse. The divergence of the cross section (34) for forward scattering ($q \to 0$) is related to the long-range behavior of the field pulse; this behavior also occurs for the Coulomb potential where the Rutherford cross section diverges in the forward direction.

We can now conclude that also the longitudinal scattering is limited to momentum transfers $\hbar q \le \hbar/h$. This is due to the large-argument asymptotics of the Bessel function in the result (34)

$$qh \gg 1: \quad qhK_1(qh) \approx \sqrt{\frac{\pi qh}{2}}\,\mathrm{e}^{-qh}\,, \tag{36}$$

giving an exponential suppression for large qh. The shot-noise field is thus also 'rough' on a scale $l_c \sim h$, and does not behave qualitatively different compared to the thermal magnetic near field.

We finally comment on our neglect of the diffusive electron motion in the wire. Since this effect gives rise to the nonzero resistivity of the wire, it is in fact included in the Johnson-noise approach for the metallic substrate. The finite drift velocity of the electrons, which makes the distribution $P(v)$ asymmetric, does not change our conclusions either because it is typically much smaller than the width of $P(v)$. The electron drift is taken into account in the spectrum shown in Fig. 6.

8 Perspectives

We have reviewed in this paper loss, heating and decoherence mechanisms for wire-based atom chips and their scaling with the microtrap geometry and the substrate-material properties. The importance of the shot-noise level for current noise has been highlighted. Using a simple model, we have shown that the spatial correlation length of magnetic fields due to shot noise is fixed by the distance between microtrap and chip wire.

The extreme miniaturization of atom-chip traps below the 1-μm scale may not be possible with 'conventional', conducting nanostructures, because magnetic field fluctuations due to thermal and technical current fluctuations become quite strong. The key process is a noise-induced change of the atomic sublevel $|m\rangle$ ('spin flip'). Its rate, which can be related to the trap lifetime, also dictates the order of magnitude of more subtle processes involving heating of the center-of-mass motion or qubit dephasing. The timescale for useful coherent manipulations is thus at least limited to a few hundred ms at a height of a few μm. Depending on the gate time of two-qubit operations, this timescale may be sufficient.

Several strategies leading to more robust atom chips can be imagined. Cooled substrates reduce thermal near-field noise, with a gain in lifetime inversely proportional to the temperature. Quiet current drivers and/or superconducting wires are an option to reduce current noise, possibly below the shot-noise level. Substrates with a permanent magnetization may also provide the required low-noise environment.

The theory of magnetic noise close to complex, magnetized structures can be developed starting from a description of the material in terms of its electric and magnetic susceptibilities. According to the fluctuation-dissipation theorem [24, 39], the imaginary parts of these fix the magnitude of the noise current and magnetization that generate thermal noise fields. This scheme can be used at low frequencies (high temperatures), which is the typical situation in atom-chip traps, but can also be extended to high frequencies where the noise reduces to vacuum fluctuations, modified by the boundary conditions set by the substrate (see e.g. [40] for a review). This kind of approach can be used to compute atom–atom interactions mediated by virtual photon exchange.

Another theoretical task is to estimate the coupling between higher atomic levels and the electric and magnetic fields originating from the surface. For example, it has been proposed to make use of the electric dipole–dipole interaction to realize controlled two-qubit gates on atom-chip traps [41, 42]. The gate operation is sped up when the atoms are excited to high-lying Rydberg states, but these states also interact strongly with the chip substrate due to their large dipole moments, hence the need for a review of their coherence times.

Finally, the understanding of the impact of the surface on the fidelity of qubit operations needs to be studied in order to optimize the construction of an atom-chip quantum processor.

ACKNOWLEDGEMENTS C.H. derived great benefit from a discussion with Marc-André Dupertuis, and thanks Sierk Pötting for his collaboration in earlier stages and for providing Fig. 1. Thanks to Johannes Hecker Denschlag for being a critical co-author in previous work. The help of Simon A. Gardiner with the numerical simulations of Fig. 4 is gratefully acknowledged. We also thank an anonymous referee for carefully reading the manuscript. This work has been supported by the Deutsche Forschungsgemeinschaft via the 'Schwerpunktprogramm Quanten-Informationsverarbeitung' and by the European Union via the ACQUIRE network (Contract No. IST-1999-11 055).

Appendix

Correlation of magnetic fields generated by shot noise

Each electron (charge e), during its passage with velocity v below the trapped atom, gives an electromagnetic 'pulse' whose vector potential is given by

$$\boldsymbol{A}(\boldsymbol{x},t)=\boldsymbol{e}_z\, e\, k(\boldsymbol{x},t-t_0;v)=\frac{\boldsymbol{e}_z\,\mu_0 ev/4\pi}{\left[x^2+y^2+(z-v(t-t_0))^2\right]^{1/2}}, \tag{A.1}$$

where the coordinates are chosen as shown in Fig. 5. The atom actually experiences an average vector potential that is due to the flow of many electrons, passing below the atom at random instants t_0. With the assumption of a stationary electron flow, we find

$$\langle \boldsymbol{A}(\boldsymbol{x},t)\rangle=-\boldsymbol{e}_z\frac{\mu_0}{4\pi}I\,\log(x^2+y^2)+\text{const.}\,, \tag{A.2}$$

where the average current is $I=e\langle n\rangle/\Delta t$ with n the number of electrons flowing during the interval Δt. This average vector potential is time-independent and gives the static magnetic field generated by the current. Note that it does not involve the velocity distribution of the electrons. (The calculation is analogous to the calculation of a photodetector current, as outlined in [43, Chapt. 9.8].)

We are interested in the correlation function of the vector potential (from which the magnetic field correlations follow via differentiation). Subtracting the average value and performing again the average over the flowing electrons, we find using the approximation of independent electrons

$$\begin{aligned}&\langle A_z(\boldsymbol{x},t+\tau)A_z(\boldsymbol{x}',t)\rangle-\langle A_z(\boldsymbol{x},t+\tau)\rangle\langle A_z(\boldsymbol{x}',t)\rangle\\&=\frac{e^2\langle n\rangle}{\Delta t}\int \mathrm{d}t'\mathrm{d}v\; P(v)k(\boldsymbol{x},t'+\tau;v)k(\boldsymbol{x}',t';v)\,,\end{aligned} \tag{A.3}$$

where the 'pulse function' $k(\dots,t;\dots)$ is defined in (A.1). The prefactor $e^2\langle n\rangle/\Delta t=eI$ is the shot-noise spectrum SN_I (10). The Fourier integral with respect to the time difference τ gives the squared Fourier transform of the pulse function that can be evaluated analytically. We do not give this formula here, but proceed directly to the magnetic field correlation tensor. After differentiation, one needs the Fourier transform

$$\int \mathrm{d}t\frac{v\,\mathrm{e}^{\mathrm{i}\omega t}}{\left[r^2+(z-vt)^2\right]^{3/2}}=\frac{2\,\mathrm{e}^{\mathrm{i}\omega z/v}|\omega/v|}{r}K_1(r|\omega/v|)\,, \tag{A.4}$$

where $r^2=x^2+y^2$ and K_1 is a Bessel function. The magnetic noise field has the same orientation (azimuthal) as the static field, so that, in cylindrical coordinates, the correlation tensor has a single nonzero element given by

$$\begin{aligned}S_{\varphi\varphi'}(\boldsymbol{x},\boldsymbol{x}';\omega)=&\frac{\mu_0^2\,SN_\mathrm{I}}{4\pi^2\,rr'}\int \mathrm{d}v\; P(v)\,\mathrm{e}^{\mathrm{i}(z-z')\omega/v}\\&\times\frac{rr'\omega^2}{v^2}K_1(r|\omega/v|)K_1(r'|\omega/v|).\end{aligned} \tag{A.5}$$

In the low-frequency limit where $\omega h,\omega r\ll v$, one gets $(r\omega/v)K_1(r\omega/v)\approx 1+\mathcal{O}((r\omega/v)^2)$. At the guide center $r=r'=h,\ z=z'$, we then recover the magnetic noise spectrum (11) with $S_\mathrm{I}(\omega)=SN_\mathrm{I}$.

The scattering cross section (28) involves the Fourier transform of the correlation function (A.5) with respect to the distance $s=z-z'$. This gives a δ-function that permits us to perform the integral over the electron velocities. At $r=r'=h$, we get

$$\int \mathrm{d}v\; P(v)\,\delta\left(\frac{\omega}{v}+q\right)\left[\frac{h\omega}{v}K_1(h|\omega/v|)\right]^2 \tag{A.6}$$

$$=\frac{|\omega|}{q^2}P(-\omega/q)[qhK_1(qh)]^2\,. \tag{A.7}$$

For the scattering process $p_\mathrm{i}\to p_\mathrm{i}+\hbar q$, $\omega=-\omega_\mathrm{fi}$ is the negative kinetic energy difference (see (26)), so that

$$-\frac{\omega}{q}=\frac{qp_\mathrm{i}+\hbar q^2/2}{Mq}\approx\frac{p_\mathrm{i}}{M}\,, \tag{A.8}$$

neglecting the recoil shift compared to the Doppler shift. This approximation yields the scattering probability (34).

REFERENCES

1 J. Fortágh, A. Grossmann, C. Zimmermann, T.W. Hänsch: Phys. Rev. Lett. **81**, 5310 (1998)
2 J. Reichel, W. Hänsel, T.W. Hänsch: Phys. Rev. Lett. **83**, 3398 (1999)
3 J. Fortágh, H. Ott, A. Grossmann, C. Zimmermann: Appl. Phys. B **70**, 701 (2000)
4 J. Reichel, W. Hänsel, P. Hommelhoff, T.W. Hänsch: Appl. Phys. B **72**, 81 (2001); selected papers of the Bonn 2000 DPG meeting
5 W. Hänsel, P. Hommelhoff, T.W. Hänsch, J. Reichel: Nature **413**, 498 (2001)
6 H. Ott, J. Fortágh, G. Schlotterbeck, A. Grossmann, C. Zimmermann: Phys. Rev. Lett. **87**, 230401 (2001); J. Fortágh, H. Ott, S. Kraft, A. Günther, C. Zimmermann: to be published in Appl. Phys. B **76** (2003) DOI 10.1007/s00340-003-1107-9
7 A.E. Leanhardt, A.P. Chikkatur, D. Kielpinski, Y. Shin, T.L. Gustavson, W. Ketterle, D.E. Pritchard: Phys. Rev. Lett. **89**, 040401 (2002)
8 S. Schneider, A. Kasper, Ch. vom Hagen, M. Bartenstein, B. Engeser, T. Schumm, I. Bar-Joseph, R. Folman, L. Feenstra, J. Schmiedmayer: submitted to Phys. Rev. A (2002) [cond-mat/0210488]; see also online bibliography at http://bec01.phy.GaSoU.edu
9 J. Reichel: Appl. Phys. B **74**, 469 (2002)
10 R. Folman, P. Krüger, J. Schmiedmayer, J.H. Denschlag, C. Henkel: In *Adv. At. Mol. Opt. Phys.*, ed. by B. Bederson, Vol. 48, (Academic, New York 2002) pp. 263–356
11 E.A. Hinds, I.G. Hughes: J. Phys. D: Appl. Phys. **32**, R119 (1999)
12 J. Schmiedmayer: Eur. Phys. J. D **4**, 57 (1998)
13 R. Grimm, M. Weidemüller, Y.B. Ovchinnikov: Adv. At. Mol. Opt. Phys. **42**, 95 (2000)
14 C. Henkel, M. Wilkens: Europhys. Lett. **47**, 414 (1999)
15 C. Henkel, S. Pötting, M. Wilkens: Appl. Phys. B **69**, 379 (1999); selected papers of the Heidelberg 1999 DPG meeting
16 J. Fortágh, H. Ott, S. Kraft, C. Zimmermann: Phys. Rev. A **66**, 041604(R) (2002)
17 A.E. Leanhardt, Y. Shin, A.P. Chikkatur, D. Kielpinski, W. Ketterle, D.E. Pritchard: submitted for publication (2002) [cond-mat/0211345]
18 J. Weiner, V.S. Bagnato, S. Zilio, P.S. Julienne: Rev. Mod. Phys. **71**, 1 (1999)
19 R. Frisch, E. Segré: Z. Phys. **75**, 610 (1933)
20 C.V. Sukumar, D.M. Brink: Phys. Rev. A **56**, 2451 (1997)
21 E.A. Hinds, C. Eberlein: Phys. Rev. A **61**, 033614 (2000); erratum: Phys. Rev. A **64**, 039902(E) (2001)
22 J.M. Wylie, J.E. Sipe: Phys. Rev. A **30**, 1185 (1984)
23 C. Cohen-Tannoudji, J. Dupont-Roc, G. Grynberg: *Processus d'Interaction Entre Photons et Atomes* (InterEditions, Paris 1988) [English translation: *Atom–Photon Interactions – Basic Processes and Applications* (Wiley, New York 1992)]
24 T. Varpula, T. Poutanen: J. Appl. Phys. **55**, 4015 (1984)
25 C. Henkel, S. Pötting: Appl. Phys. B **72**, 73 (2001); selected papers of the Bonn 2000 DPG meeting
26 Q.A. Turchette, D. Kielpinski, B.E. King, D. Leibfried, D.M. Meekhof, C.J. Myatt, M.A. Rowe, C.A. Sackett, C.S. Wood, W.M. Itano, C. Monroe, D.J. Wineland: Phys. Rev. A **61**, 063418 (2000)
27 A. Stern, Y. Aharonov, Y. Imry: Phys. Rev. A **41**, 3436 (1990)
28 T.A. Savard, K.M. O'Hara, J.E. Thomas: Phys. Rev. A **56**, R1095 (1997)
29 M.E. Gehm, K.M. O'Hara, T.A. Savard, J.E. Thomas: Phys. Rev. A **58**, 3914 (1998)
30 W.H. Zurek: Phys. Today, 36 (October 1991)
31 E.A. Hinds, C.I. Vale, M.G. Boshier: Phys. Rev. Lett. **86**, 1462 (2001)
32 E. Andersson, T. Calarco, R. Folman, M. Andersson, B. Hessmo, J. Schmiedmayer: Phys. Rev. Lett. **88**, 100401 (2002)
33 M. Olshanii: Phys. Rev. Lett. **81**, 938 (1998)
34 A. Görlitz, J.M. Vogels, A.E. Leanhardt, C. Raman, T.L. Gustavson, J.R. Abo-Shaeer, A.P. Chikkatur, S. Gupta, S. Inouye, T. Rosenband, W. Ketterle: Phys. Rev. Lett. **87**, 130402 (2001)
35 S. Dettmer, S. Dettmer, D. Hellweg, P. Ryytty, J.J. Arlt, W. Ertmer, K. Sengstock, D.S. Petrov, G.V. Shlyapnikov, H. Kreutzmann, L. Santos, M. Lewenstein: Phys. Rev. Lett. **87**, 160406 (2001)
36 D.S. Petrov, G.V. Shlyapnikov, J.T.M. Walraven: Phys. Rev. Lett. **87**, 050404 (2001)
37 C. Henkel, S.A. Gardiner: submitted for publication (2002) [cond-mat/0212415]
38 C. Henkel, K. Joulain, R. Carminati, J.-J. Greffet: Opt. Commun. **186**, 57 (2000)
39 G.S. Agarwal: Phys. Rev. A **11**, 230 (1975)
40 L. Knöll, S. Scheel, D.-G. Welsch: In *Coherence and Statistics of Photons and Atoms*, ed. by J. Perina (Wiley, New York 2001)
41 T. Calarco, E.A. Hinds, D. Jaksch, J. Schmiedmayer, J.I. Cirac, P. Zoller: Phys. Rev. A **61**, 022304 (2000)
42 G.K. Brennen, I.H. Deutsch, P.S. Jessen: Phys. Rev. A **61**, 062309 (2000)
43 L. Mandel, E. Wolf: *Optical Coherence and Quantum Optics* (Cambridge University Press 1995)